Research Paper

Bioassay for monitoring the anti-aging effect of cord blood treatment

Sang-Hun Bae[1*], Ala Jo[1,2*], Jae Hyun Park[1], Chul-Woo Lim[1], Yuri Choi[1], Juhyun Oh[2], Ji-Min Park[1], TaeHo Kong[1], Ralph Weissleder[2,3], Hakho Lee[2✉], Jisook Moon[1✉]

1. Department of Biotechnology, College of Life Science, CHA University, Gyeonggi-do 13488, Republic of Korea
2. Center for Systems Biology, Massachusetts General Hospital, Harvard Medical School, Boston, MA 02114, USA
3. Department of Systems Biology, Harvard Medical School, Boston, MA 02115, USA

*These authors contributed equally.

✉ Corresponding author: Hakho Lee, PhD. Center for Systems Biology, Massachusetts General Hospital, 185 Cambridge St, CPZN 5206, Boston, MA 02114, USA. 617-726-8226 hlee@mgh.harvard.edu Jisook Moon, PhD. Department of Biotechnology, College of Life Science, CHA University, Pangyo-ro 335, Bundang-gu, Seongnam-si, Gyeonggi-do 13488, Republic of Korea. 82-31-881-7210 jmoon@cha.ac.kr

Abstract

Background: Treating aged animals with plasma of an early developmental stage (e.g, umbilical cord plasma) showed an impressive potential to slow age-associated degradation of neuronal and cognitive functions. Translating such findings to clinical realities, however, requires effective ways for assessing treatment efficacy; ideal methods should be minimally invasive, amenable for serial assays, cost-effective, and quantitative.

Methods: We developed a new biosensor approach to monitor anti-aging therapy. We advanced two key sensor components: i) a blood-borne metabolite was identified as a surrogate aging-marker; and ii) a compact and cost-effective assay system was developed for on-site applications. We treated aged mice either with human umbilical cord plasma or saline; unbiased metabolite profiling on mouse plasma revealed arachidonic acid (AA) as a potent indicator associated with anti-aging effect. We next implemented a competitive magneto-electrochemical sensor (cMES) optimized for AA detection directly from plasma. The developed platform could detect AA directly from small volumes of plasma (0.5 μL) within 1.5 hour.

Results: cMES assays confirmed a strong correlation between AA levels and anti-aging effect: AA levels, while decreasing with aging, increased in the plasma-treated aged mice which also showed improved learning and memory performance.

Conclusions: The cMES platform will empower both pre- and clinical anti-aging research by enabling minimally invasive, longitudinal treatment surveillance; these capacities will accelerate the development of anti-aging therapies, improving the quality of individual lives.

Key words: Anti-aging, Arachidonic acid, Metabolite profiling, Magneto-electrochemical sensor, Biosensor

Introduction

Aging is increasingly recognized as a clinical risk factor for cognitive degeneration (e.g., neurodegeneration, dementia) and other chronic diseases (e.g., cancer, cardiovascular disease, muscular degeneration) [1]. With expanding human lifespan and growing elderly population, significant efforts are underway to elucidate aging mechanism [1–3] and to find therapeutic strategies to slow down or even reverse aging processes [4]. Indeed, promising results from animal studies have been reported; adult mice that received plasma transfusion from young mice regained cognitive function, synaptic plasticity, and neuronal activity [5]. Rapid development in anti-aging treatments and their translation into

human trials are anticipated [6]. Current metrics to monitor treatment effects, however, have limited practicality, as methods are often difficult to apply with human (e.g., invasive brain imaging, controlled behavior observation) and subjective (e.g., questionnaires on patient experiences). One key requisite in advancing anti-aging therapies thus lies in developing quantitative, minimally invasive assays for treatment monitoring.

We reasoned that metabolites would be a potent source for anti-aging biomarkers. Metabolites are an essential phenotype in an organism and are being studied as diagnostic biomarkers for other diseases [7]. In particular, aging is typically associated with metabolic changes or dysfunction, which affects overall metabolite profiles in organisms. As such, it is conceivable that tracing the composition and/or levels of metabolites would inform the efficacy of anti-aging treatment. Furthermore, metabolite assays, particularly in the form of blood tests, could be quantitative and minimally invasive; these merits would facilitate apprising different treatment regimens or patient groups, and monitoring (anti-)aging dynamics through serial sampling.

We herein describe a new biosensor strategy for monitoring anti-aging treatment. Two key elements were advanced: i) a blood-borne metabolite was identified as a surrogate aging-marker; and ii) a fast, cost-effective assay system was developed for applications in routine clinical settings. Specifically, we treated a cohort of aged mice (about 2 years old) with plasma from human cord blood. Comprehensive metabolomics analyses on mouse blood revealed that arachidonic acid (AA), whose level significantly decreased with aging, reversely increased in the treated group. This observation led us to devise a magneto-electrochemical sensor for small molecular targets: we optimized a competitive electrochemical reaction wherein AA was captured on magnetic beads and concentrated for higher sensitivity. The developed platform could detect AA directly from small volumes of plasma (0.5 µL) within 1.5 hour. Using this platform, we could further establish a positive correlation between blood AA levels and animals' better performance in the motor task.

Results

Treating adult mice with cord blood plasma

Figure 1a shows the overall experiment scheme. As an anti-aging agent, we used plasma derived from human umbilical cord blood samples. Previous studies showed that aged mice that were injected with young mouse plasma recovered spatial memory function, and systemic administration of human cord blood plasma improved hippocampal-dependent cognition in aged mice [5, 8]. Injecting plasma, which is devoid of cellular components, minimized the risk of immune rejection coming from species mismatch. Aged mice (starting age, 18 month old) were randomized and received either plasma (a treatment group) or saline buffer (a sham group) via tail-vain injection (130 µL; see **Fig. S1** for details). As a positive control, young mice (3 month old) were used. Plasma derived from umbilical cord blood was not pooled and each mouse was repeatedly infused with plasma from the same donor (**Fig. S1**). Following a 4-week treatment, mice were subject to a behavior test (i.e., rotarod), and blood was drawn for analyses.
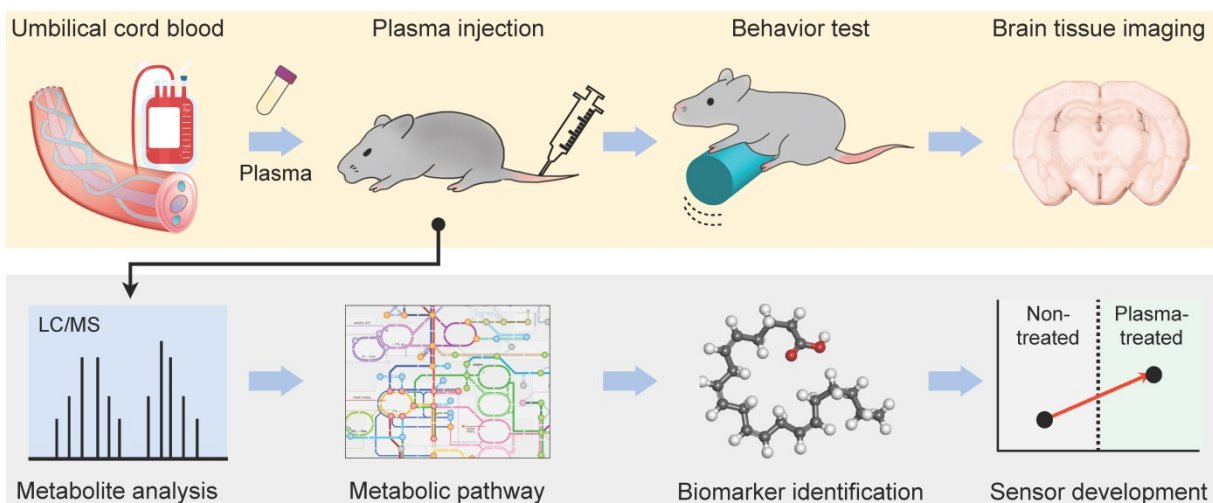
Figure 1. Experimental design. Human cord blood plasma was administered to the young (3-month-old), old (20- and 23-month-old) and plasma-treated old groups (20- and 23-month-old). The three groups were subjected to 2-trial Rotarod tests to measure motor coordination and learning. Untargeted metabolite profiling was performed on blood from the three groups, and the most anti-aging relevant pathway was determined through a bioinformatic approach. The biosensor was developed to detect the most important metabolite of the pathway.
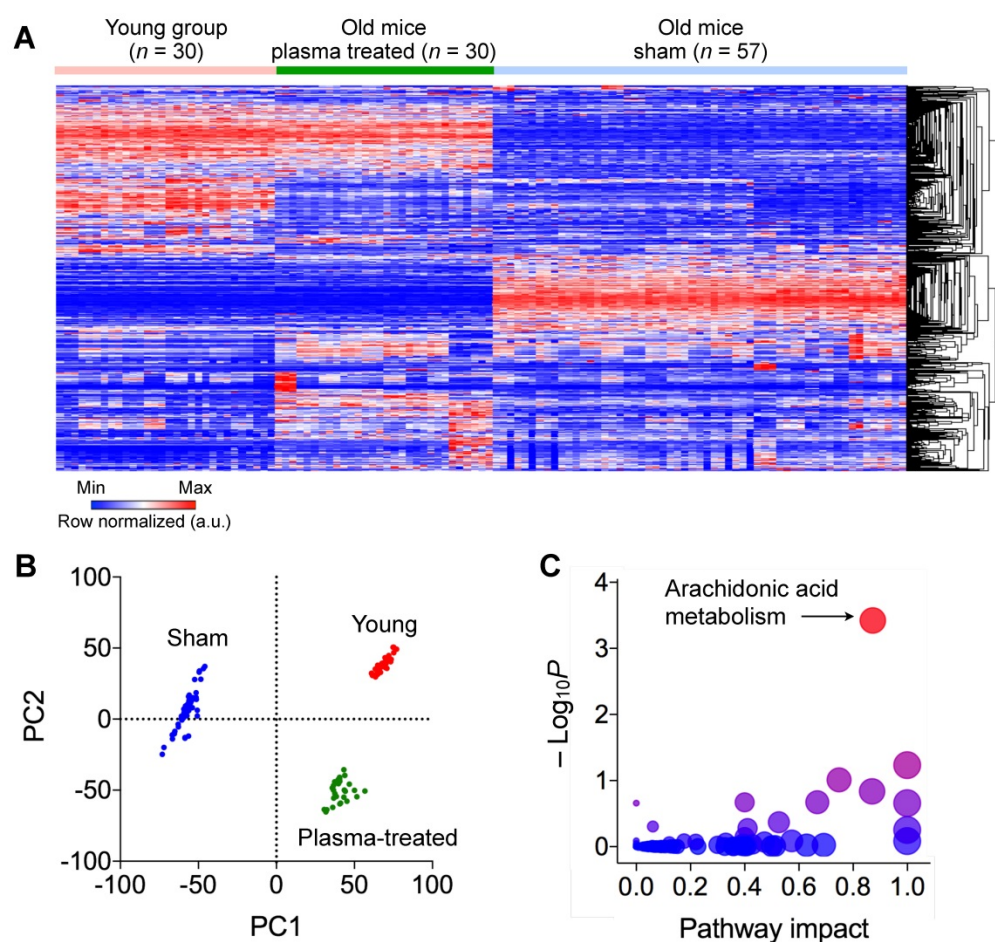
Figure 2. Determination of metabolite biomarkers associated with human cord blood plasma treatment. (A) Global profile of metabolite perturbation. Rows correspond to features (a unique combination of m/z value and retention time) from LC/MS and columns to samples. Rows are hierarchically clustered. **(B)** Score plot of PCA for dimensional reduction. Samples were plotted against the principal component (PC) 1 and 2. Values in parentheses of axis legends are proportions of variance explained by those components. PC1 most likely explains anti-aging effects, given that the plasma treated group was much closer to the young group than to the sham group. **(C)** Pathway enrichment analysis. Metabolites were identified by matching the measured m/z values to molecular mass information. Each circle represents a specific pathway found. For a given pathway, the x location or size of the circle corresponds to relative-betweeness centrality (a measure of pathway impact) of metabolites, and the y location or color (lower *p* values for red and higher for blue) to the extent to which metabolites are over-represented. Dominant pathways have higher x and y values. Accordingly, arachidonic acid (AA) metabolism was identified as the most probable pathway for explaining the anti-aging effects of the cord blood plasma.

Metabolic analyses on mouse blood samples

We first performed an unbiased small-molecule metabolite profiling in mouse plasma. Blood samples from all three mouse groups were subjected to liquid chromatography and mass spectrometry (LC/MS) analyses. We processed the m/z data by MAIT (metabolite automatic identification toolkit) and identified statistically significant features via ANOVA (8572 unique combinations of m/z and retention time) (**Fig. 2a**). Hierarchical clustering analysis (HCA) of metabolites revealed two key patterns: i) metabolite profiles were distinctively different between aged (non-treated) and young mice; and ii) the profile of plasma-treated aged mice were closer to that of young mice.

Principal component analysis (PCA) revealed inherent structures of metabolomics data (**Fig. 2b**). About 50 percent of total variations were explainable by the first (PC1) and the second principal components (PC2). All three cohorts (i.e., young, plasma-treated, and sham groups) settled at discrete positions, indicating that biologically relevant features for differentiating group classes were identified. Interestingly, the plasma-treated aged group moved away from the sham toward the young group. To quantify the group separation, we computed hierarchical clustering on the two principal components. In the dendrogram, the young and plasma-treated groups were clustered at a lower dissimilarity level (or a higher similarity level, 1120.9) than the non-treated group (3162.5) (**Fig. S2**). These results indicate that selected features (variables or rows in **Fig. 2a**) can be used to infer metabolite biomarker relevant to aging and anti-aging. We annotated the features with known metabolites using a database in the public domain [9].

We further assessed functions and inter-connectivity of the identified metabolites, applying KEGG (Kyoto Encyclopedia of Genes and Genomes) [10] mapping. For a given pathway, we measured i) the over-representation of a candidate metabolite and ii) its importance (i.e., betweenness centrality) [11] as a key intermediate node between pairs of other metabolites (see Methods for details). We found that arachidonic acid (AA) metabolism was the most over-represented pathway (the highest y-value in **Fig. 2c**), and metabolites in that pathway tended to locate at communication paths (higher x-values in **Fig. 2c**) and govern information flow. Among many metabolites in AA metabolism, we selected AA itself as a biomarker; as a starting entry into the pathway, AA alone can be a representative of other perturbed metabolites.

## Competitive magneto-electrochemical sensor (cMES) for AA detection in plasma

We next set out to advance a fast, onsite assay system for AA detection. We opted to use the magneto-electrochemical sensing technology [12–17]. It combines target enrichment and detection into a single platform: magnetic beads (MBs) are used to capture and label molecular targets, and bead-bound targets are detected through electrochemical sensing. This approach has many practical advantages: i) native samples (plasma or blood) can be directly used without the need for sample purification; ii) the assay achieves high detection sensitivity through magnetic enrichment and enzymatic signal amplification; iii) based on the electrical detection scheme, sensors can be easily miniaturized as a portable device (**Fig. 3a**).

Detecting AA through the magneto-electrochemical sensing, however, posed a technical challenge; since AA is a small molecule (~304.5 Da), immunoassays using a pair of AA-antibodies were difficult to apply. We thus explored a competitive assay format (cMES; competitive magneto-electrochemical sensor) that required only a single AA antibody (**Fig. 3b**). For target capture, we coated MBs with AA-antibodies (MB_{Ab}). We also prepared a competing agent (AA-HRP) by conjugating AA with an oxidizing enzyme (horseradish peroxidase, HRP). Specifically, we used a hapten form; AA conjugated on bovine serum albumin (BSA), and further conjugated HRP to the BSA carrier (**Fig. S3**). For the cMES assay, blood samples were mixed with MB_{Ab} and AA-HRP. The amount of AA-HRP was enough to saturate the AA-binding sites in MB_{Ab} (Methods). This would lead to differential HRP-loading on MBs, depending on the endogenous AA amounts in samples. Sequentially adding a chromogenic electron mediator (3,3′,5,5′-tetramethylbenzidine, TMB) generated an electrical current that was read out by a planar electrode. The reaction time for AA capture and TMB incubation was optimized to maximize the signal level (**Fig. S4**).
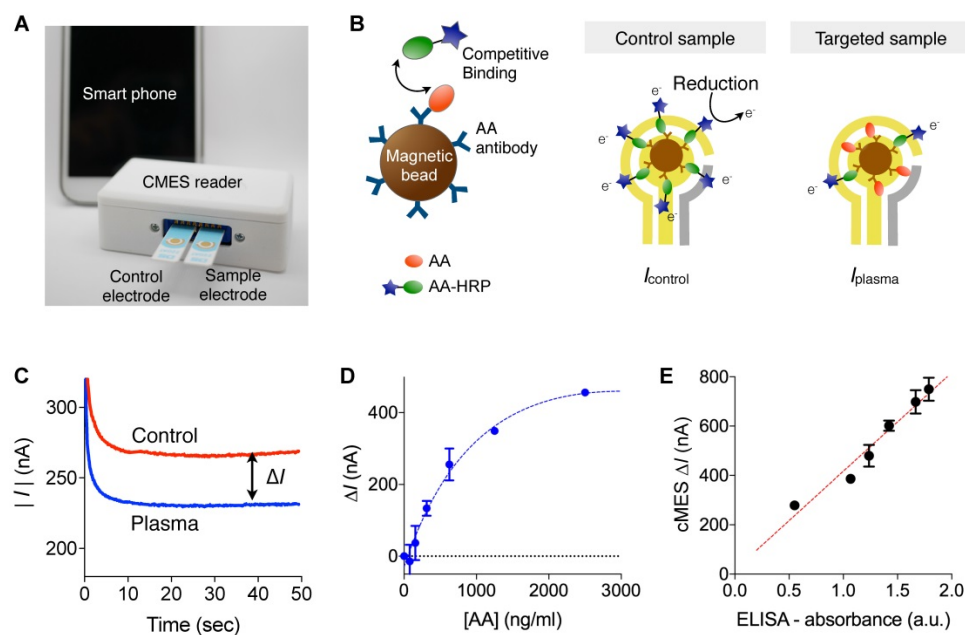
Figure 3. Competitive magneto-electrochemical sensor (cMES) for AA assay. (A) Device schematic. The cMES device has a small footprint and affords on-site operations. **(B)** We devised a competitive electrochemical assay for AA detection. Magnetic beads (MB_{Ab}) were conjugated with antibodies against AA. Control samples contained AA-HRP only and were mixed with magnetic beads. Test samples were mixed with magnetic beads and AA-HRP. **(C)** Electrical currents measured by the portable cMES reader. In the cMES assay, the current magnitude decreases with increasing AA concentration [AA]. The signal from the control sample set the baseline for [AA] = 0 ng/mL. The current difference (ΔI) between the control and the targeted plasma samples was used as an analytical metric. **(D)** Known amounts of AA were spiked in serum and measured by the cMES. The limit of detection was ~ 126 ng/mL. (E) cMES and ELISA were compared for concordance. The results from both modalities showed a good agreement (R^2 = 0.959). Data are displayed as mean ± SEM from triplicate measurements.
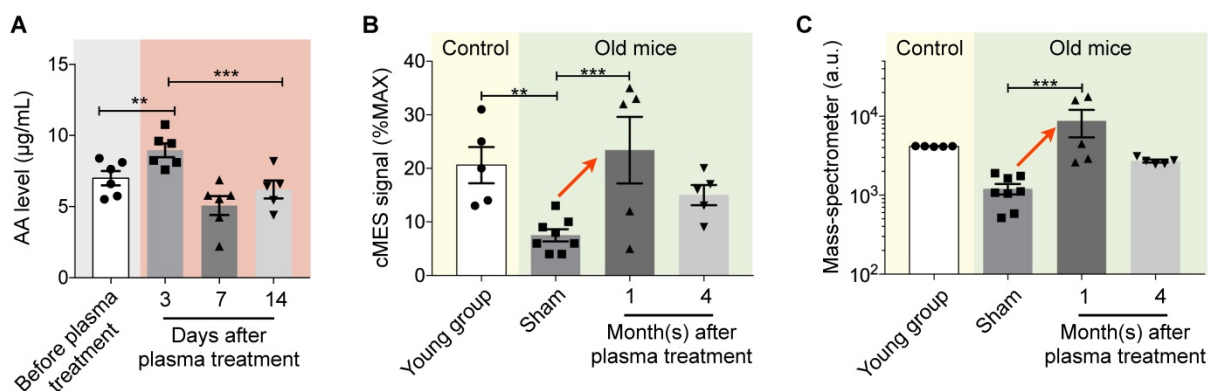
Figure 4. AA measurements in plasma samples. (A) Time course analysis of mouse AA level after plasma injection. We injected 130 μL of plasma (AA concentration = 7.2 μg/mL) into mice ($n = 6$) and collected mice blood after 3, 7 and 14 days. AA levels of mice blood were then monitored. AA levels significantly increased at day 3 and returned to the normal level after 7 days. *$p < 0.05$; **$p < 0.01$; ***$p < 0.001$. **(B)** Mouse plasma samples were assayed. In the control group ($n = 5$), young mice (ages, 5 and 8 months) had higher AA levels than sham-treated old mice (ages, 20 and 23 months; $n = 8$). For the plasma-treated group ($n = 5$), sustained increase in AA was observed. *$p < 0.05$; **$p < 0.01$; ***$p < 0.001$. **(C)** Plasma samples from the same cohorts as in (b) were analyzed by mass spectrometry. The AA levels showed a similar trend as measured by cMES. *$p < 0.05$; **$p < 0.01$; ***$p < 0.001$. Data are displayed as mean ± SEM.

As a result of competitive assay, the magnitude of the electrical current decreased with higher plasma AA concentrations ([AA]). We therefore prepared a control sample by incubating MB$_{Ab}$ with AA-HRP only. The control sample was used to set the upper baseline (i.e., [AA] = 0 ng/mL) for calculating signal differences; electrical currents from control and plasma sample were measured, and the net difference $|\Delta I| = |I_{control} - I_{plasma}|$ was obtained (**Fig. 3c**). Such differential measurements also compensated for common background signal.

The titration experiment (**Fig. 3d**) using samples spiked with varying amounts of AA revealed the limit of detection (LOD) as ~125.9 ng/mL. The LOD of assay was ~300-fold lower than the typical AA concentration of (38 μg/ml) in young mice plasma (5 months, $n = 2$). Based on these results, we diluted initial plasma samples (100-fold) by adding a buffer solution (see Methods). Signal from nonspecific binding was close to an intrinsic background level (~43 nA), potentially benefiting from the high dilution factor. We also confirmed that the assay results matched with those from conventional ELISA ($R^2 = 0.961$, **Fig. 3e**). The cMES assay, however, was faster (1 hour) than ELISA (4 hours), mostly due to the fast binding kinetics; in the cMES, MBs capture AA in the entire sample volume (3-dimensional diffusion), whereas AA capture relies on 1-dimensional diffusion in the plate-based ELISA.

AA monitoring in plasma-treated mice

We applied cMES to analyze AA levels in mice after a single plasma treatment. Since AA is naturally present in human cord blood, plasma injection would additively increase mouse AA levels. The average AA concentration from six different human cord blood plasma was 7.2 ± 0.5 μg/mL (mean ± SEM). We injected 130 μL of human cord blood plasma to mice ($n = 6$) and monitored their AA levels (**Fig. 4a**). Plasma injection immediately increased blood AA levels (day 3; $p < 0.01$, compared to all other time points), but the effect was temporary; AA levels returned to normal 7 days after treatment ($p = 0.34$, compared to the time point before plasma injection).

We next monitor plasma AA levels after the full treatment schedule (**Fig. S1**). Three different mouse cohorts were used: a plasma-treated ($n = 8$) and a sham ($n = 8$) aged groups (20-23 months old), and a young control group (<8 months old, $n = 5$). We used 0.5 μL of mouse plasma for each measurement. The sham group showed lower AA level compared to the young group ($p = 0.003$, **Fig. 4b**). The plasma treated group, however, showed increased AA levels even after 1 month after the treatment. The effect was sustained up to 4 months post treatment; the plasma-treated group had higher AA level than the sham group ($p = 0.0003$). We also analyzed aliquots of samples via LC/MS (**Fig. 4c**). The results from both assays were concordant, corroborating AA's value as a biomarker.

Plasma treatment leading to cognitive and behavior improvement in aged mice

We further assessed behavioral phenotypes of animal cohorts, particularly evaluating their motor learning and memory functions. We performed 2-trial rotarod tests at 1 and 4 months after plasma or sham treatment (**Fig. 5a**); the latency (running time) of a mouse before falling off on a rotating rod was used to assess animal's motor performance. At 1 month after treatment (20-month-old), the latency of both the sham and the plasma-treated groups was significantly lower ($p < 0.0001$) than that of the young (5-month-old) group (**Fig. 5b**). The plasma-treated

group, however, showed a gradual improvement in the motor learning and memory, whereas the same faculty declined in the sham group. Changes in AA levels proceeded behavior changes, which could serve as an early indicator of anti-aging treatment effect (**Fig. 5c**).

Brain tissue analyses (**Figs. 5d, 5e**) showed that aged mice (the sham group) had smaller area of DCX-positive cells in the sub-ventricular zone than young mice. Conversely, the area of DCX-positive cells increased in the plasma-treated animal and remained unchanged (p = 0.04) indicating that injected cord blood plasma stimulated neurogenesis of old brain. The results suggest the potential benefit of plasma treatment on sustained neurogenesis which resulted in improved motor function in the treated group.

Discussion

Advances in rejuvenation therapies concomitantly increase the need for an objective and quantitative measure to read out the treatment efficacy. We thus designed our study to identify molecular biomarkers that can best explain phenotypic features of aging and anti-aging treatment. Our animal experiments led to the following observations: i) metabolite profiles of young and adult mouse cohorts are evidently different; and ii) injecting human cord plasma into aged mice changes their metabolite patterns closer to those of young mice. Interestingly, we found arachidonic acid (AA) as the most effective surrogate biomarker for

anti-aging treatment; AA metabolism was highly unregulated both in young and plasma-treated mice, and was found playing key roles in interacting with other metabolic pathways such as linoleic acid metabolism [10, 18].

We further developed a fast, portable sensor system (cMES) to facilitate AA detection in routine research and clinical settings. We specifically integrated a competitive assay scheme with immunomagnetic enrichment in a bid to detect small molecular targets (i.e., metabolites) directly from plasma samples. This combination brings in the following advantages. (i) The assay benefits from fast binding kinetics, since magnetic beads capture AA in the entire sample volume (3-dimensional diffusion). (ii) Assay processes (e.g., washing steps) are simplified with external magnets used for bead collection. (iii) By magnetically concentrating AA-bound beads near the detection electrode, the overall analytical signal can be improved (~72%) [12]. Indeed, we showed that the cMES assay uses <1 μL of plasma with the total assay time within 1.5 hour. Both cMES and mass spectrometry consistently showed that plasma AA levels decrease with aging, but that they reversely increase with cord-plasma treatment. Importantly, increases in AA levels could be an early indicator of improved cognitive functions in treated animals. These results highlight the utility of AA-cMES; with minimally invasive blood draw, individual patients can be monitored in a serial fashion to better assess treatment efficacy.
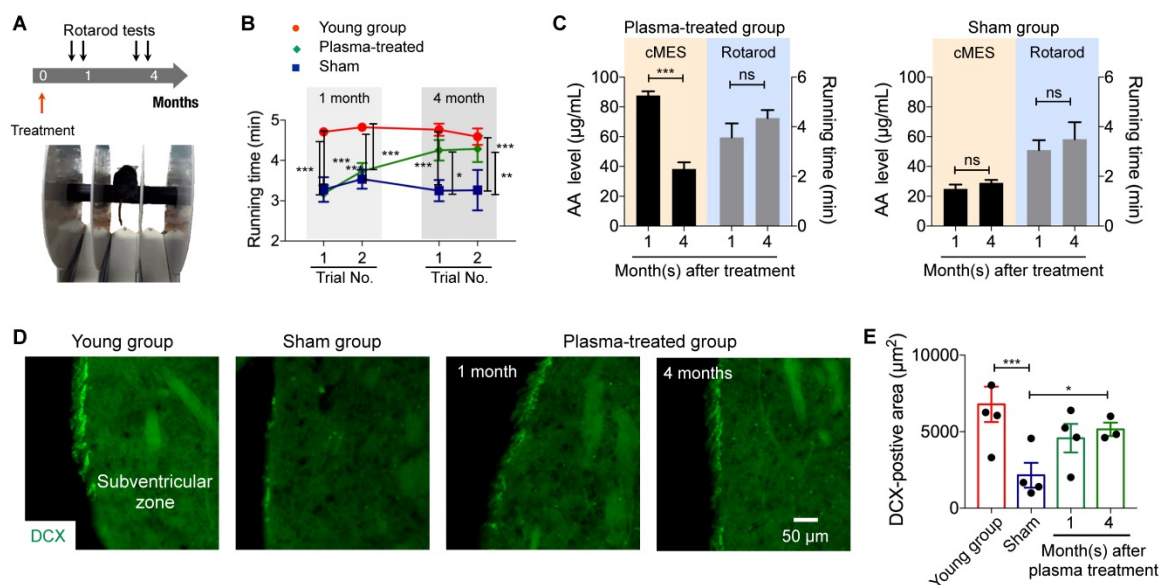
Figure 5. Behavioral and molecular assays. (A) 2-trial Rotarod tests were conducted at 1 and 4 months after plasma injection. **(B)** The plasma-treated group showed progressive improvement in motor coordination; the performance was close to that of the young group in the end (the second trial at 3 months). The running time of the sham group decreased with aging. *p < 0.05; **p < 0.01. **(C)** For the plasma treated group, increase in AA levels preceded the motor function improvement. *p < 0.05; **p < 0.01; ***p < 0.001. **(D)** Brain cells in the subventricular zone were immunostained for a neurogenesis marker, doublecortin (DCX). Scale bar is 50 μm. Note that the sham group had significant smaller area of DCX-positive cells in the sub-ventricular zone than young mice, whereas the area increased in the plasma-treated animal and remained unchanged. **(E)** The area of DCX-positive cells in image (D) was measured. *p < 0.05; ***p < 0.001.

AA has been shown to promote muscle growth and brain development [19, 20]. Other reports also highlighted the potential benefits of AA in anti-aging [21, 22]. The current study is in line with these findings, but its scope was limited to establishing a correlative relation between AA levels and anti-aging phenotypes. Serial AA monitoring, however, indicated that AA increases in plasma-treated mice was likely from endogenous sources, not from transfused plasma. Moreover, sustained anti-aging effects were observed in recipient mice even 4 months after the end of plasma treatment. The motor learning and the memory functions improved; and the number of neuronal precursor cells increased in brain. These observations strongly suggest physiological changes in plasma-treated mice; the exact mechanism has yet to be elucidated.

Several other limitations of this study should be addressed in future research. First, the cMES assay needs to be refined for higher accuracy. In particular, with the lack of true negative samples (i.e., blood samples without any endogenous AA), it was difficult to account for signals from non-specific binding. Conceivably, the effect of blood matrices may be negligible as we diluted samples by 100-fold. Such an assumption, however, is to be validated by using AA-deleted plasma samples that could be prepared from an AA-deficient mouse model [23] or through immunodepletion of AA. Second, we focused on detecting a single metabolite in AA metabolism for simplicity, but this approach may ignore biological context such as interactions between metabolites in a given pathway. Including a panel of metabolites would better capture metabolic perturbations and also increase the diagnostic accuracy. cMES can be easily scaled to detect diverse markers while consuming small sample amounts. Third, interpolating current findings to humans would be challenging. Although mice and humans share similar metabolic pathways, mice has 7-fold higher metabolic rate than humans [24]. Human trials are necessary to determine optimal plasma doses for infusion and to set baselines for biomarkers; informed by animal studies, we are planning such human studies. These efforts will accelerate the development of anti-aging therapies, improving the quality of individual lives as well as reducing societal burdens.

Methods

Experimental design

Plasma was separated from human umbilical cord blood collected at delivery. The cord blood plasma was administered by intravenous infusion to old mice (18-month-old), and sham control (18-month-old) and young mice (3-month-old as positive control) was injected with saline. At 1 and 4 months after the transplantation, 2-trial rotarod tests were conducted to assess motor coordination and long-term memory (**Fig. S1**). The untargeted metabolite profiling was performed on the blood from the three groups and bioinformatical analysis determined the anti-aging relevant pathway (Arachidonic acid metabolism). The biosensor was developed for detecting blood-circulating arachidonic acid easily and efficiently.

Cord blood sample preparation

Human cord blood was collected under Institutional Review Board of the CHA General Hospital (Seoul, Korea, IRB No. CHAMC-2015-08-130-009). Human cord blood was donated from 4 donors and treated with citrate-phasphate-dextrose with adenine (CPDA-1) anticoagulant. Human cord blood plasma was isolated by centrifugation at 2,000 g for 15 min at room temperature. Isolated plasma samples were stored at -80°C and used with a single freeze-thaw cycle at room temperature.

Animal experiments

Animal protocols were approved by the CHA University Institutional Animal Care and Use Committee (IACUC). We used 18-month-old female C57BL/6 mice to evaluate metabolic perturbations and behavioral phenotypes that correlate with aging and anti-aging. The positive controls were 3-month-old female C57BL/6 mice. All mice were bred at room temperature in standard 12 hours light-dark cycle. For the adult mice, the cord blood plasma or saline (130 µL) was intravenously injected 12 times for 4 weeks. Isolated human cord blood plasma was not pooled, and a given animal received cord blood plasma from the same donor. The number of animals used in each experiment is described in the corresponding method sections. Plasma was collected via centrifugation (3,000 g, 15 min at room temperature).

Metabolite acquisition and data analysis

For profiling of blood-borne metabolites, blood was collected from the mice by cardiac puncture at the designated time points: the young group (3-month-old, n = 10), the sham group (20-month-old, n = 10; 23-month-old, n = 12), the plasma-treated group (20-month-old, n = 5; 23-month-old, n = 5). The blood samples were analyzed using a liquid chromatography-mass spectrometry (LC-MS) system (Agilent). We converted LC/MS files into a standard mzXML format (ProteoWizard) [25] and then processed them using MAIT (metabolite automatic identification toolkit) [26] for feature detection,

statistical analysis, and metabolite identification. Statistically significant features (i.e., ionized and/or fragmented metabolites) were identified via analysis of variance (ANOVA). These features were matched to all possible putative metabolites in metabolome database [9] based on the mass/charge ratio of the mass spectral ion (m/z tolerance of 0.005). We characterized global metabolite alterations via hierarchical clustering analysis and the inherent structures of metabolomics data via principal component analysis (PCA). Two or three technical replicates (ensuring that technical variation is much smaller than biological variation) per mouse were included in the unsupervised learning such as PCA and hierarchical clustering. Hierarchical clustering on principal components (HCPC) was performed by FactoMineR, an R package [27]. For a functional analysis, the most likely metabolic pathways to be perturbed by aging and plasma treatment were determined via KEGG pathway analysis (MetaboAnalyst 3.0) [28]. Hypergeometric distribution was used to measure the over-representation of the matched metabolites in specific KEGG pathways.

Preparation of immunomagnetic beads

Magnetic beads (5 mg) coated with epoxy groups (Dynabeads M-270 Epoxy, Invitrogen) were suspended in 100 µL of 0.1 M sodium phosphate solution. One hundred micrograms of antibody against arachidonic acid (Biomatik) was added and mixed thoroughly. One hundred microliters of 3 M ammonium sulfate solution was added, and the mixture was incubated at room temperature for 2 hours and then further incubated at 4 ℃ for overnight with slow tilt rotation. The conjugation reaction was carried out at pH = 7.4. These processes induce the formation of covalent bonding between epoxy (bead) and amine (antibody) groups, which we previously confirmed by subjecting antibody-bead conjugates to pH challenges [29]. On average 2.4×10^4 antibodies were immobilized per bead. Antibody-conjugated magnetic beads were separated with a permanent magnet, washed twice with PBS solution, and resuspended in 200 µL of PBS with 1% BSA. Beads were stored in 4 ℃ up to one month.

HRP conjugation to arachidonic acid

HRP was then conjugated to BSA via reductive amination chemistry. Specifically, 100 µg of BSA-conjugated AA (RPU51089, Biomatik) was dissolved in 0.5 mL of 0.2 M carbonate-biocarbonate buffer (pH 9.4), added to one milligram of lyophilized EZ-link Plus Activated Peroxidase (Thermo Scientific), and incubated for 1 hour at room temperature. Next, 10 µL of sodium cyanoborohydride (Thermo Scientific) was added and the mixture was incubated for 15 min at room temperature. Finally, 20 µL of Quenching buffer (Thermo Scientific) was added, followed by 15 min incubation at room temperature. Gel electrophoresis and protein band analysis confirmed HPR conjugation to BSA-AA (**Fig. S3a**). HRP-conjugated AA were collected and concentrated with Amicon Ultra 100K centrifugal filter (Millipore). Remaining peroxidase and BSA-AA were washed-out with PBS for four times.

Electrochemical detection of AA in plasma samples

For electrochemical detection of AA, blood was collected from the young (n = 5), sham (n = 8), and plasma-treated groups (n = 5 for 1 month and n = 5 for 3 months). Mouse plasma samples (0.5 µL) were diluted in 50 µL of 1% BSA in PBS (×100-fold dilution) and mixed with immunomagnetic bead solution (50 µL) and HRP-conjugated AA solution (50 µL). The amount of AA-HRP was large enough to saturate the binding sites in magnetic beads. We used about 8.4×10^7 beads per test, which made available 2.0×10^{12} AA-binding sites. The amount of AA-HRP was $\sim 1.7 \times 10^{13}$; the ratio between AA-HRP and binding sites was ~8:1. The mixture was incubated at room temperature for 1 hour with slow tilt rotation. The control bead was prepared by mixing 1% BSA in PBS (50 µL) with immunomagnetic bead solution (50 µL) and HRP-conjugated AA solution (50 µL). All reacted beads were separated with a permanent magnet and washed twice with 80 µL of PBS (1% BSA). Finally, the beads were resuspended in 7 µL of PBS. The prepared bead solution and 20 µL of TMB solution (Biomatik) were loaded on top of the electrode. After 6 min, chronoamperometry measurement was started. We used a miniaturized electrochemical sensor (a prototype system developed by AcurreHealth Inc.). The current levels in the range of 40-45 s were averaged. We used the conversion factor (×100) to report the estimated original AA concentrations in plasma.

Enzyme-linked immunosorbent assay (ELISA)

ELISA experiments were performed using mouse arachidonic acid (AA) ELISA kit (Biomatik) according to the manufacturing guidelines. Serially diluted AA were added into each well, and incubated with HRP-conjugated AA at 37 ℃ for 40 min. After washing with washing buffer for four times, TMB solution was added and incubated for 20 min. The color development was stopped by adding stop solution. The absorbance was read at 450 nm using

microplate reader (Tecan).

Rotarod test

We modified the Rotarod test of Kong et al. [30] to assess locomotor coordination. The rotarod with a 3-cm diameter rod started at 4 rpm and accelerated by 4 rpm per 30 seconds for 5 min. The mice were placed on the rod, and the time taken for the mice to fall off the rod was measured. Each mouse was given 3 trials a day, and the running times of each day were calculated as the average of the training times. The first rotarod test was conducted at 1-month post plasma treatment: the young group (n = 29), the sham group (n = 17), the plasma-treated group (n = 22). A retraining session was started at 4-months post plasma treatment. To avoid over-training, retraining was conducted for 2 days. The other procedure was the same as the first session.

Brain tissue imaging

On 1 month (n = 4) and 4 months (n = 3) after injection of human cord blood plasma or saline injection, animals were euthanized and then perfused with 4% paraformaldehyde (PFA) and PBS through the left ventricle. The young (n = 5) and sham groups (n = 4) were used as controls. Their brains were extracted and cryoprotected. Each brain was sectioned on a cryotome at a thickness of 30 μm. To perform the immunohistochemistry, non-specific binding was blocked with 5% normal goat serum in 0.3% Triton X-100 for 40 min. Primary antibody against Doublecortin (DCX; 1:400, Cell Signaling, #4604S) was applied overnight at 4 °C, and then PBS was used for washing [31]. Secondary antibody Alexa Fluor 488 (1:2000, Invitrogen, #A11008) was used for detection of DCX. Images were taken using a fluorescence microscope (Nikon Eclipse 80i) and analyzed using Image J [32].

Statistical analysis

Statistical analysis was performed using R basic functions and lme4, an R package for either Linear Mixed-Effects Models or Generalized Linear Model (GLM) followed by an LSD post-hoc test [33]. Data are presented as the means ± standard error and a p value of < 0.05 was considered significant.

Supplementary Material

Supplementary figures.
http://www.thno.org/v09p0001s1.pdf

Competing Interests

The authors have declared that no competing interest exists.

References

1. Wyss-Coray T. Ageing, neurodegeneration and brain rejuvenation. Nature. 2016; 539: 180-6.
2. Prasad S, Sung B, Aggarwal BB. Age-associated chronic diseases require age-old medicine: role of chronic inflammation. Prev Med. 2012; 54 Suppl: S29-37.
3. Barzilai N, Cuervo AM, Austad S. Aging as a Biological Target for Prevention and Therapy. JAMA. 2018; 320: 1321-2.
4. Lopez-Otin C, Blasco MA, Partridge L, Serrano M, Kroemer G. The hallmarks of aging. Cell. 2013; 153: 1194-217.
5. Castellano JM, Mosher KI, Abbey RJ, McBride AA, James ML, Berdnik D et al. Human umbilical cord plasma proteins revitalize hippocampal function in aged mice. Nature. 2017; 544: 488-92.
6. de Cabo R, Carmona-Gutierrez D, Bernier M, Hall MN, Madeo F. The search for antiaging interventions: from elixirs to fasting regimens. Cell. 2014; 157: 1515-26.
7. Johnson CH, Ivanisevic J, Siuzdak G. Metabolomics: beyond biomarkers and towards mechanisms. Nat Rev Mol Cell Biol. 2016; 17: 451-9.
8. Villeda SA, Luo J, Mosher KI, Zou B, Britschgi M, Bieri G et al. The ageing systemic milieu negatively regulates neurogenesis and cognitive function. Nature. 2011; 477: 90-4.
9. Wishart DS, Feunang YD, Marcu A, Guo AC, Liang K, Vazquez-Fresno R et al. HMDB 4.0: the human metabolome database for 2018. Nucleic Acids Res. 2018; 46: D608-17.
10. Okuda S, Yamada T, Hamajima M, Itoh M, Katayama T, Bork P et al. KEGG Atlas mapping for global analysis of metabolic pathways. Nucleic Acids Res. 2008; 36: W423-6.
11. Koschutzki D, Schreiber F. Centrality analysis methods for biological networks and their application to gene regulatory networks. Gene Regul Syst Bio. 2008; 2: 193-201.
12. Jeong S, Park J, Pathania D, Castro CM, Weissleder R, Lee H. Integrated Magneto-Electrochemical Sensor for Exosome Analysis. ACS Nano. 2016; 10: 1802-9.
13. Park J, Lin HY, Assaker JP, Jeong S, Huang CH, Kurdi T et al. Integrated Kidney Exosome Analysis for the Detection of Kidney Transplant Rejection. ACS Nano. 2017; 11: 11041-6.
14. Lewis JM, Vyas AD, Qiu Y, Messer KS, White R, Heller MJ. Integrated Analysis of Exosomal Protein Biomarkers on Alternating Current Electrokinetic Chips Enables Rapid Detection of Pancreatic Cancer in Patient Blood. ACS Nano. 2018; 12: 3311-20.
15. de la Escosura-Muñiz A, Maltez-da Costa M, Sánchez-Espinel C, Díaz-Freitas B, Fernández-Suarez J, González-Fernández Á et al. Gold nanoparticle-based electrochemical magnetoimmunosensor for rapid detection of anti-hepatitis B virus antibodies in human serum. Biosens Bioelectron. 2010; 26: 1710-4.
16. Krause CE, Otieno BA, Bishop GW, Phadke G, Choquette L, Lalla RV et al. Ultrasensitive microfluidic array for serum pro-inflammatory cytokines and C-reactive protein to assess oral mucositis risk in cancer patients. Anal Bioanal Chem. 2015; 407: 7239-43.
17. Sánchez-Tirado E, Salvo C, González-Cortés A, Yáñez-Sedeño P, Langa F, Pingarrón JM. Electrochemical immunosensor for simultaneous determination of interleukin-1 beta and tumor necrosis factor alpha in serum and saliva using dual screen printed electrodes modified with functionalized double-walled carbon nanotubes. Anal Chim Acta. 2017; 959: 66-73.
18. Hanna VS, Hafez EAA. Synopsis of arachidonic acid metabolism: A review. J Adv Res. 2018; 11: 23-32.
19. Markworth JF, Cameron-Smith D. Arachidonic acid supplementation enhances in vitro skeletal muscle cell growth via a COX-2-dependent pathway. Am J Physiol Cell Physiol. 2013; 304: C56-67.
20. Hadley KB, Ryan AS, Forsyth S, Gautier S, Salem N, Jr. The Essentiality of Arachidonic Acid in Infant Development. Nutrients. 2016; 8: 216.
21. Das UN. Ageing: Is there a role for arachidonic acid and other bioactive lipids? A review. J Adv Res. 2018; 11: 67-79.
22. Yu Y, Li T, Wu N, Ren L, Jiang L, Ji X et al. Mechanism of Arachidonic Acid Accumulation during Aging in Mortierella alpina: A Large-Scale Label-Free Comparative Proteomics Study. J Agric Food Chem. 2016; 64: 9124-34.
23. Fan YY, Monk JM, Hou TY, Callway E, Vincent L, Weeks B et al. Characterization of an arachidonic acid-deficient (Fads1 knockout) mouse model. J Lipid Res. 2012; 53: 1287-95.
24. Demetrius L. Of mice and men. When it comes to studying ageing and the means to slow it down, mice are not just small humans. EMBO Rep. 2005; 6 Spec No: S39-44.

25. Chambers MC, Maclean B, Burke R, Amodei D, Ruderman DL, Neumann S et al. A cross-platform toolkit for mass spectrometry and proteomics. Nat Biotechnol. 2012; 30: 918-20.

26. Fernandez-Albert F, Llorach R, Andres-Lacueva C, Perera A. An R package to analyse LC/MS metabolomic data: MAIT (Metabolite Automatic Identification Toolkit). Bioinformatics. 2014; 30: 1937-9.

27. Le S, Josse J, Husson F. FactoMineR: An R Package for Multivariate Analysis. J Stat Softw. 2008; 25: 1-18.

28. Xia J, Sinelnikov IV, Han B, Wishart DS. MetaboAnalyst 3.0--making metabolomics more meaningful. Nucleic Acids Res. 2015; 43: W251-7.

29. Min J, Nothing M, Coble B, Zheng H, Park J, Im H et al. Integrated Biosensor for Rapid and Point-of-Care Sepsis Diagnosis. ACS Nano. 2018; 12: 3378-84.

30. Kong T, Park JM, Jang JH, Kim CY, Bae SH, Choi Y et al. Immunomodulatory effect of CD200-positive human placenta-derived stem cells in the early phase of stroke. Exp Mol Med. 2018; 50: e425.

31. Bae SH, Kong TH, Lee HS, Kim KS, Hong KS, Chopp M et al. Long-lasting paracrine effects of human cord blood cells on damaged neocortex in an animal model of cerebral palsy. Cell Transplant. 2012; 21: 2497-515.

32. Jensen EC. Quantitative analysis of histological staining and fluorescence using ImageJ. Anat Rec (Hoboken). 2013; 296: 378-81.

33. Bates D, Mächler M, Bolker B, Walker S. Fitting Linear Mixed-Effects Models Using lme4. J Stat Softw. 2015; 67: 1-48.